Optics Communications 385 (2017) 78–86

Contents lists available at ScienceDirect

Optics Communications

journal homepage: www.elsevier.com/locate/optcom

Adaptive variable selection for extended Nijboer–Zernike aberration retrieval via lasso

Bin Wang[a,b], Huai-An Diao[a,*], Jianhua Guo[a,*], Xiyang Liu[c], Yuanhao Wu[b]

[a] School of Mathematics and Statistics, Northeast Normal University, No. 5268 Renmin Street, Changchun 130024, China
[b] Changchun Institute of Optics, Fine Mechanics and Physics, Chinese Academy of Sciences, Changchun 130033, China
[c] School of Computer Science and Technology, Xidian University, Xi'an 710071, China

ARTICLE INFO

Keywords:
Wave-front sensing
Phase retrieval
Active or adaptive optics

ABSTRACT

In this paper, we propose extended Nijboer–Zernike (ENZ) method for aberration retrieval by incorporating lasso variable selection method which can improve the accuracy of aberration retrieval. The proposed model is computed by the state-of-art algorithm of the Bregman iterative algorithm (Bregman, 1967 [1]; Cai et al., 2008 [2]; Yin et al., 2008 [3]) for L_1 minimization problem with adaptive regularized parameter choice based on the strategy (Ito et al., 2011 [4]). Numerical simulations for real world and simulated phase data validate the effectiveness of the proposed ENZ AR via lasso.

1. Introduction

Parameter estimation based aberration retrieval methods using focal plane images usually adopt Zernike polynomials to represent aberration linearly. In 2002, an extended Nijboer–Zernike (ENZ) diffraction which is based on Debye diffraction approximation and the Zernike expansion of generalized pupil function was introduced, providing an analytic description of the focal field over a large volume and realizable solutions for the aberration coefficients [5,6]. For the cases of high numerical aperture (NA) and large Fresnel number (FN), the ENZ approach agree well with the more rigorous Rayleigh–Sommerfeld-I (RSI) diffraction integral providing that enough expansion terms are used for approximation [7], and was incorporated into the Ignatowsky–Richards/Wolf formalism for the vectorial treatment [8,9].

Dirksen et al. [10] proposed an ENZ aberration retrieval (AR) to identify lens imperfections from the intensity point spread function (PSF) of the optical system, which has been subsequently applied in the field of high resolution optical lithography, where the optical defects of the projection lens can be derived from recorded point source images in a photoresist layer [11]. Moreover, ENZ AR was applied to estimate optical path aberrations in telescopes, particularly non-common path aberrations of NACO adaptive optics in very large telescopes (VLTs) [12]. Antonello and Verhaegen [13] considered combining convex optimization methods with the ENZ theory for phase retrieval.

The AR process is an inverse problem based on diffraction and statistical parameter estimation. The aberration is usually linearly represented by Zernike expansions, where the variables are the Zernike coefficients. In principle, Zernike expansions have infinite terms, but in practice, only the first Q terms are retained for ENZ AR assuming that the truncated terms can be neglected, where Q is defined empirically over a given range. The estimation variance increases with respect to the number of Zernike terms, whereas a small number of terms would truncate some large coefficients, enhancing the bias and hence increasing the mean square error (MSE). The detailed explanations for the above phenomena can be found in [14, pp. 156–159].

Selecting the important terms of Zernike polynomials is difficult and important. For example, Q=45 was chosen to estimate NACO non-common path aberrations [12]. When the real and imaginary parts of the NZ coefficients are viewed as different variables, there are 89 variables for Q=45, because the first term of ENZ coefficient only has real value. However, as shown in Fig. 4 in [12], most coefficients of these 89 variables, say 67%, are near to 0. Thus, the sparsity of the expansion coefficients should also be considered in the physical modeling and numerical computation. The sparsity of the expansion coefficients is a key feature in the proposed AR model (Section 3). Moreover, van Haver and Janssen [15] proved that the generalized pupil function expressed by ENZ is convergent, which means that the coefficients of the ENZ expansions tend to zero when the number of terms increases. This is the theoretical foundation for the sparsity property of ENZ expansion coefficients.

In the following, we adopt the methodology of the paper [16] to justify that the parameter vector formed by ENZ coefficients is sparse. We use randomized wavefronts to investigate the distribution of the

* Corresponding authors.
E-mail addresses: hadiao@nenu.edu.cn (H.-A. Diao), jhguo@nenu.edu.cn (J. Guo).

http://dx.doi.org/10.1016/j.optcom.2016.10.033
Received 20 July 2016; Received in revised form 12 October 2016; Accepted 16 October 2016
Available online 26 October 2016

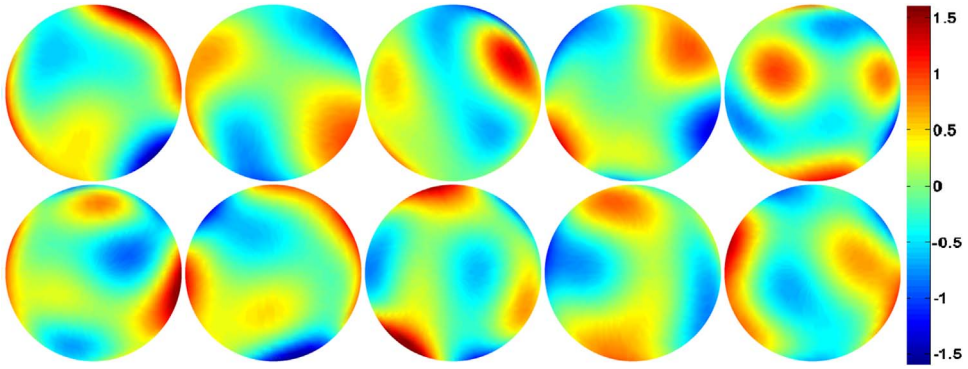

Fig. 1. Some simulated random phases.

expansion coefficients qualitatively. Wavefronts were simulated using the method in [17] to generate 1000 random phases by first 21 terms of Frits Zernike expansion, where the phase should satisfy the following requirement $pv < 2\pi$, $rms = 0.2\pi$ (rad). Here we explain the above requirement in detail. In the paper [17], the ratio D/r_0 should be predetermined, where D is the diameter of the telescope, and r_0 is atmospheric coherent length. For the given ratio D/r_0, the corresponding *rms* of the wavefront can be determined. In fact, the above mechanism can be realized by pre-determining the values of *rms*. For the reason to choose $pv < 2\pi$, we want to avoid the occurrence of phase wrapping. When the phase wrapping happens, more coefficients of ENZ are needed to fit the wavefront. Some of wavefronts are shown in Fig. 1. These phases at constant amplitude generated 1000 generalized pupils, which were then expressed by ENZ via (2.1) by choosing the parameter Q=91 in ENZ. We refer to [13, Appendix], for the detailed deduction of the relationship between the Zernike coefficients and the ENZ coefficients. Separating the real and imaginary parts of each coefficients, thus each generalized pupil has 181 coefficients. For 1000 generalized pupils, we count those 181 000 coefficients and draw their histogram to estimate the priori distribution of the coefficients via ENZ, see Fig. 2a. The x-axis denotes the values of 181 000 coefficients, while the y-axis represents the percentage of the same values of 181 000 coefficients. As shown in the figure, the histogram peaks at zero and falls off much faster than the counterparts of standard Gaussian distribution. For example, the coefficients of less than 0.01 are about 60% of the total coefficients, and the coefficients of less than 0.1 are a bit more than 91% of the total coefficients, which means that the sparsity of the coefficients via ENZ should be taken into account during ENZ aberration retrieval. Moreover, we characterize the distributions of 181 000 coefficients in terms of the shape of their logarithm, as shown in Fig. 2b. The logarithms of the probabilities shown in the y-axis of Fig. 2a are plotted in blue color. Also, we plot the logarithm of the probability density function of the standard Gaussian and Laplacian distribution in green and dark color, respectively. As shown in Fig. 2b, the logarithmic histogram peaked at zero and falls off much faster than the standard Gaussian distribution, even faster than Laplacian distribution in the log domain. This kind of distribution is usually called “sparse”.

Variable selection is where variables with high correlations to the observation data are preferentially chosen. It can solve the problem with sparse prior. Some common methodologies for variable selection are cross validation, hypothesis testing, and regularization [18]. Regularization using the least absolute shrinkage and selection operator (lasso) was introduced by Tibshirani [19], which can capture important features of the model without training sets. Lasso can be efficiently solved by considering data sparsity. The lasso estimates linear regression coefficients through L_1-constrained least squares. Noting the form of the L_1-constrained term in lasso, Tibshirani suggested that lasso estimates can be interpreted as posterior mode estimates when the regression parameters have Laplacian priors [19].

In this paper, by incorporating lasso variable selection into ENZ AR (lasso ENZ AR), we can improve the accuracy of the estimation through utilizing a large number of ENZ AR and trading off the terms adaptively with respect to those coefficients which approach 0. This produces a dynamically adaptive variable selection strategy in the ENZ AR process. The proposed lasso ENZ AR can be computed efficiently via the state-of-art algorithm of the Bregman iterative algorithm [1–3] for L_1 minimization problem with adaptive regularized parameter choice based on the strategy [4].

The paper is organized as follows. ENZ AR is reviewed in Section 2. The lasso ENZ AR algorithm is developed in Section 3, and simulations for ENZ AR and lasso ENZ AR are performed in Section 4. Final conclusions are summarized in Section 5.

2. Aberration retrieval using extended Nijboer–Zernike diffraction

2.1. Extended Nijboer–Zernike diffraction

The generalized pupil function can be expressed using Nijboer–

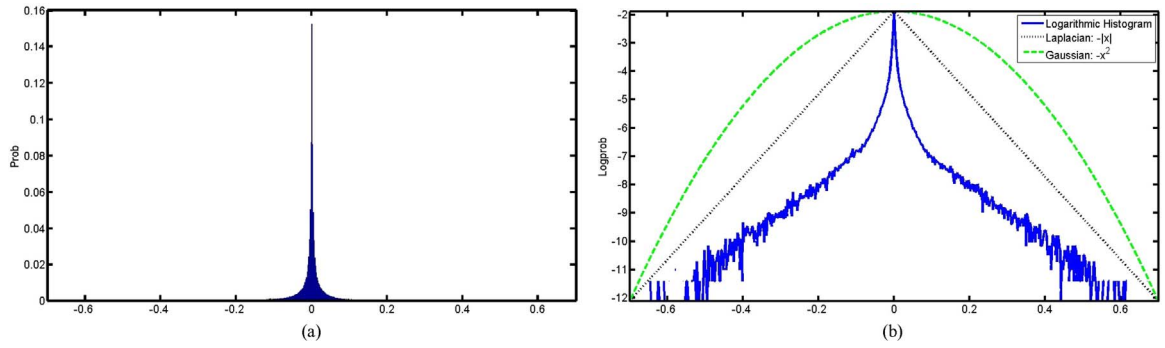

Fig. 2. The distributions of the ENZ coefficients. (a) Histogram. (b) Logarithmic histogram. (For interpretation of the references to color in this figure caption, the reader is referred to the web version of this paper.)

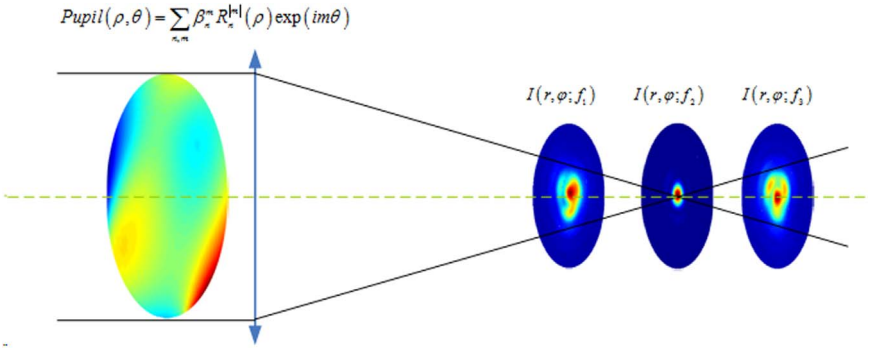

Fig. 3. Generalized pupil and through focus light fields can be linearly expanded by combinations of $\{\beta_n^m\}$ coefficients. The measured through focus PSFs are inputs for estimating $\{\beta_n^m\}$.

Zernike coefficients [20] as

$$Pupil(\rho,\theta)=\sum_{n,m}\beta_n^m R_n^{|m|}(\rho)\exp(\mathbf{i}m\theta), \tag{2.1}$$

where $\{\beta_n^m\}$ are coefficients of the Nijboer–Zernike expansions; m and n are integers such that $n\geq 0$, $n-|m|$ is even and $n-|m|\geq 0$. The first $\beta_0{}^0$ is real, and $\beta_n{}^m$ is complex for $m\neq 0$, $b\neq 0$.

Let us introduce a variable vector, $\boldsymbol{\beta}$, to denote the coefficients $\{\beta_n^m\}$ in (2.1), which is used to denote an unknown variable vector to estimate aberration in Section 2.2. Given a non-negative increasing integer sequence, q, the integers m, n in (2.1) can be viewed functions of q, denoted by gn: $q\rightarrow n$, gm: $q\rightarrow m$, so the qth element of $\boldsymbol{\beta}$ is $\beta_{gn(q)}^{gm(q)}$. For example, for the 22th element of $\boldsymbol{\beta}$, $n=6$, $m=-4$, and for the 35th element of $\boldsymbol{\beta}$, $n=7$, $m=7$. Indeed, $n=gn(q)$ is an increasing function of q, whereas this is not true for $m=gm(q)$.

The radial polynomials in (2.1) are [11,20]:

$$R_n^{|m|}(\rho)=\sum_{s=0}^{\frac{n-|m|}{2}}(-1)^s\frac{(n-s)!}{s!\left(\frac{n+|m|}{2}-s\right)!\left(\frac{n-|m|}{2}-s\right)!}\rho^{n-2s}. \tag{2.2}$$

Thus, $R_n^{|m|}(\rho)$ can be constructed before aberration retrieval for a specific choice of m, n, and ρ. *Pupil* is a linear function of $\beta_n{}^m$. The light field on the focal plane can be expressed as [6]:

$$U(r,\varphi;f)=2\sum_{n,m}\mathbf{i}^m\beta_n^m V_n^m(r,f)\exp(\mathbf{i}m\varphi), \tag{2.3}$$

where $f=\frac{\pi NA^2}{\lambda}z=\frac{2\pi}{\lambda}\frac{z}{8(F\#)^2}$, where NA is the numerical aperture, $F\#$ is the F-number, and z is the defocus distance, λ is the wavelength, and (r,φ) are polar coordinates on the image plane. The Bessel series [5]

$$V_n^m(r,f)=\exp(\mathbf{i}f)\sum_{l=1}^{\infty}(-2\mathbf{i}f)^{l-1}\sum_{j=0}^{p}v_{lj}\frac{J_{|m|+l+2j}(2\pi r)}{l(2\pi r)^l}, \tag{2.4}$$

where J_m is a Bessel function of the first kind with order m, and

$$v_{lj}=(-1)^{\frac{n-m}{2}}(|m|+l+2j)\binom{|m|+j+l-1}{l-1}\binom{j+l-1}{l-1}\binom{l-1}{p-j}/\binom{q+l+j}{l}, \tag{2.5}$$

where $q=\frac{n+|m|}{2}$, $p=\frac{n-|m|}{2}$, and $l=1,2,\ldots;j=0,\ldots,p$.

2.2. The ENZ AR modeling

From (2.3), the PSF intensity in the focal region can be expressed as

$$I(r,\varphi;f)=|U(r,\varphi;f)|^2=4|V_0^0(r,f)|^2(\beta_0^0)^2+8\beta_0^0\sum_{n,m}{}'Re[\beta_n^m\mathbf{i}^m V_n^m(r,f)V_0^{0*}(r,f)\exp(\mathbf{i}m\varphi)]+C(r,\varphi;f)=4|V_0^0(r,f)|^2(\beta_0^0)^2+8\beta_0^0\sum_{n,m}{}'Re(\beta_n^m)Re[\mathbf{i}^m V_n^m(r,f)V_0^{0*}(r,f)]\cos(m\varphi)-8\beta_0^0\sum_{n,m}{}'Re(\beta_n^m)Im[\mathbf{i}^m V_n^m(r,f)V_0^{0*}(r,f)]\sin(m\varphi)-8\beta_0^0\sum_{n,m}{}'Im(\beta_n^m)Re[\mathbf{i}^m V_n^m(r,f)V_0^{0*}(r,f)]\sin(m\varphi)-8\beta_0^0\sum_{n,m}{}'Im(\beta_n^m)Im[\mathbf{i}^m V_n^m(r,f)V_0^{0*}(r,f)]\cos(m\varphi)+C(r,\varphi;f), \tag{2.6}$$

where

$$C(r,\varphi;f)=4\sum_{n_1,m_1;n_2,m_2}{}''Re\{\beta_{n_1}^{m_1}\beta_{n_2}^{m_2*}\mathbf{i}^{m_1-m_2}V_{n_1}^{m_1}V_{n_2}^{m_2*}\exp[\mathbf{i}\varphi(m_1-m_2)]\}, \tag{2.7}$$

are the remaining second order cross terms, $'$ means omission of n=0 terms in the sum, $''$ means omission of $n_1=m_1=0$ or $n_2=m_2=0$ terms in the sum, and $Re\{\}$ denotes the real part of a complex number.

The calculated PSF intensity in the focal region, $I(r,\varphi;f)$, is used to estimate coefficients $\{\beta_n^m\}$ using (2.6), as shown in Fig. 3. The ENZ AR process, which was previously proposed in [10,12,21], has four main steps:

(1) Input the collected PSFs I_b. Set the maximum iteration step K, $I^{(0)}=I_b$, $C^{(0)}=0$ and k=0.
(2) Assume that $I^{(k)}$ can be described as linear combinations of the entrance pupil aberrations $\{\beta_n^m\}$. This is equivalent to omitting the cross terms of (2.6). And then estimate $\{\beta_n^m\}^{(k)}$.
(3) Calculate $C^{(k+1)}$ using (2.7) by $\{\beta_n^m\}^{(k)}$.
(4) Set $I^{(k+1)}=I_b-C^{(k+1)}$, $k=k+1$. If $k>K$, exit. Else go to (2).

The extended ENZ AR algorithm (extended ENZ AR) of ENZ AR [10] was proposed in [21], and its detailed descriptions are listed in Algorithm 1.

Algorithm 1. Extended ENZ AR.

Input: the collected PSFs I_b, the maximum iteration step K
Output: the variable vector $\hat{\boldsymbol{\beta}}^{(K)}$
Main Procedure:
1: **Initialization:**
2: Set $C^{(0)}=0$;
3: Using (A.23), (A.27), (A.30) and (A.33), calculate **W**.
4: Using (A.25), (A.29), and (A.30), calculate **H**.
5: **M** = **WH**.
6: **for** $k=0,1,2,\ldots K$ **do**
7: $I_d^{(k)}\leftarrow I_b-C^{(k)}$.

8: Create $\mathbf{z}^{(k)}$ from $I_d^{(k)}$ by (A.22), (A.26), and (A.30).
9: $\mathbf{L}^{(k)} = \mathbf{W}\mathbf{z}^{(k)}$.
10: $\widehat{\boldsymbol{\beta}}^{(k)} \leftarrow (\mathbf{M}^T\mathbf{M})^{-1}\mathbf{M}^T\mathbf{L}^{(k)}$.
11: Using (2.7), calculate $C^{(k+1)}$.
12: **end for**

3. Extended Nijboer–Zernike aberration retrieval variable selection via lasso

3.1. Variable selection via lasso

As reviewed in Section 1, variable selection is the process of selecting a subset of relevant variables for use in model construction. Lasso has been shown to be an efficient method for variable section, and so we incorporate lasso into ENZ AR.

First, let us review some well-known results on the linear model [18]. Suppose we have a linear model

$$\mathbf{A}\mathbf{x} + \boldsymbol{\delta} = \mathbf{y}, \tag{3.1}$$

where $\mathbf{A} = (\mathbf{A}_0, \mathbf{A}_2, \ldots, \mathbf{A}_{Q-1})$ are N-vectors representing the covariates and $\mathbf{y}$ is the vector of responses for N samples. We can always assume that the covariates have been standardized to have mean 0 and unit length by location and scale transformations, and that the response has mean 0. The noise vector, $\boldsymbol{\delta}$, satisfies $\boldsymbol{\delta} \sim N(0, \sigma^2\mathbf{I}_N)$, and I_N is an N-dimension identity matrix. Thus,

$$\sum_{i=0}^{N-1} \mathbf{y}_i = 0, \quad \sum_{i=0}^{N-1} \mathbf{A}_{ij} = 0, \quad \sum_{i=0}^{N-1} \mathbf{A}_{ij}^2 = 1. \tag{3.2}$$

Lasso [18] is a constrained version of ordinary least squares (OLS) [19] and estimates $\mathbf{X}$ by the optimization

$$\hat{\mathbf{x}} = \arg\min_{\mathbf{x}} \| \mathbf{A}\mathbf{x} - \mathbf{y} \|_2^2, \quad \mathbf{s.t.} \ \| \mathbf{x} \|_1 \le t, \tag{3.3}$$

where t is a predefined parameter. Lasso tends to shrink OLS coefficients toward 0, more so for small values of t [22]. Thus lasso can provide a better variable selection than OLS.

For the numerical method for lasso, firstly note that (3.3) can be transformed to an unconstrained optimization problem

$$\hat{\mathbf{x}} = \arg\min_{\mathbf{x}} \left\{ F(\mathbf{x}; \mathbf{y}) = \frac{1}{2} \| \mathbf{A}\mathbf{x} - \mathbf{y} \|_2^2 + J(\mathbf{x}) \right\}, \tag{3.4}$$

where $J(\mathbf{x}) = \mu \| \mathbf{x} \|_1$ is convex and non-differentiable, μ is a regularization parameter to trade off model accuracy $\| \mathbf{A}\mathbf{x} - \mathbf{y} \|_2^2$ with $\| \mathbf{x} \|_1$ which enforces the sparsity of $\mathbf{x}$. Usually, μ can be determined by some classical criteria, such as discrepancy [23,24], heuristic rules [4,25] or an adaptive method [4]. Many algorithms have been proposed to solve lasso, such as iterative reweighed least squares (IRLS) [26], least angle regression (LARS) [22], and the Bregman iterative algorithm [1–3], which is equivalent to augmented Lagrangian iteration [27,28] and has been established in [3]. In this paper, we adopt the Bregman iterative algorithm to solve the proposed lasso ENZ AR. The Bregman iterative algorithm [3] for (3.4) can be described as follows: set the initial vector $\mathbf{y}^{(0)} = \mathbf{y}$, for $k = 0, 1, 2, \ldots, do$

$$\mathbf{x}^{(k+1)} \leftarrow \arg\min_{\mathbf{x}} F(\mathbf{y}; \mathbf{y}^{(k)}), \tag{3.5}$$

$$\mathbf{y}^{(k+1)} \leftarrow \mathbf{y} + (\mathbf{y}^{(k)} - \mathbf{A}\mathbf{x}^{(k+1)}). \tag{3.6}$$

Let us briefly describe the key idea of the Bregman iterative algorithm. Firstly, the Bregman distance [3] induced by a convex function $J(\cdot)$ is defined as

$$D_J^{\mathbf{p}}(\mathbf{u}, \mathbf{v}) = J(\mathbf{u}) - J(\mathbf{v}) - \langle \mathbf{p}, \mathbf{u} - \mathbf{v} \rangle, \quad \text{where } \mathbf{p} \in \partial J(\mathbf{v})$$

where $\partial J(\mathbf{v})$ denotes the set of subdifferential of J at $\mathbf{v}$. Because $D_J^{\mathbf{p}}(\mathbf{u}, \mathbf{v}) \neq D_J^{\mathbf{p}}(\mathbf{v}, \mathbf{u})$, $D_J^{\mathbf{p}}(\mathbf{u}, \mathbf{v})$ is not a distance in the usual sense. Yet, it measures the closeness between $\mathbf{u}$ and $\mathbf{v}$ in the sense that $D_J^{\mathbf{p}}(\mathbf{u}, \mathbf{v}) \ge 0$, and $D_J^{\mathbf{p}}(\mathbf{u}, \mathbf{v}) \ge D_J^{\mathbf{p}}(\mathbf{w}, \mathbf{v})$ for any point $\mathbf{w}$ being a convex combination of $\mathbf{u}$ and $\mathbf{v}$. Instead of solving (3.4) with the constrains, in the following alternative version of each Bregman iteration, a problem in the form of

$$\min_{\mathbf{x}} D_J^{\mathbf{p}}(\mathbf{x}, \mathbf{z}) + \frac{1}{2} \| \mathbf{A}\mathbf{x} - \mathbf{d} \|_2^2 \tag{3.7}$$

is solved, and the iteration is

$$\mathbf{x}^{(k)} \leftarrow \text{solve (3.7) with } \mathbf{p} := \mathbf{p}^{(k-1)}, \quad \mathbf{z} := \mathbf{x}^{(k-1)}, \quad \mathbf{d} := \mathbf{y}, \tag{3.8}$$

$$\mathbf{p}^{(k)} \leftarrow \mathbf{p}^{(k-1)} + \mathbf{A}^T(\mathbf{y} - \mathbf{A}\mathbf{x}^{(k-1)}), \tag{3.9}$$

for $k = 1, \ldots$ starting $\mathbf{x}^{(0)} = \mathbf{0}$ and $\mathbf{p}^{(0)} = \mathbf{0}$. In (3.8) the Bregman distance $D_J^{\mathbf{p}}(\mathbf{x}, \mathbf{y})$ is introduced to be regarded as the regularized version of $J(\mathbf{x})$ and in (3.9), $\mathbf{p}^{(k)}$ is determined by the optimality condition of (3.8):

$$\mathbf{0} \in \partial J(\mathbf{x}^{(k-1)}) - \mathbf{p}^{(k-1)} + \mathbf{A}^T(\mathbf{A}\mathbf{x}^{(k-1)} - \mathbf{y}),$$

which gives update (3.9). Assuming that (3.5) and (3.8) are computed exactly, one can verify that, for all iterations k, iterations (3.5) and (3.6) and (3.8) and (3.9) are equivalent through the identity $\mathbf{p}^{(k)} = \mathbf{A}^T(\mathbf{y}^{(k)} - \mathbf{A}\mathbf{x}^{(k)})$; see Theorem 3.1 of [3]. Subproblem (3.5) can be efficiently solved by state-of-art algorithms such as gradient projection for sparse reconstruction (GPSR) [29], fixed-point continuation (FPC) [30], sparse reconstruction by separable approximation (SpaRSA) [31], etc. In this paper, we adopt SpaRSA to solve (3.5), see [31] for details. The SpaRSA utilizes the proximity operator [31] to regularize the nondifferential functional $J(\cdot)$, i.e., in the each iteration, it has the following step:

$$\mathbf{x}^{(k+1)} \to \arg\min_{\mathbf{z}} \frac{1}{2} \| \mathbf{z} - \mathbf{v}^{(k)} \|_2^2 + \frac{1}{\alpha_k} J(\mathbf{z}),$$

where $\mathbf{v}^{(k)} = \mathbf{x}^{(k)} - \frac{1}{\alpha_k}\mathbf{A}^T(\mathbf{A}\mathbf{x}^{(k)} - \mathbf{y})$ and α_k is some positive real number. This form is considered frequently in the literature, often under the name of iterative shrinkage/thresholding (IST) algorithms [31].

3.2. ENZ AR via lasso

Before we apply lasso in ENZ AR, the covariate matrix columns should be standardized to have zero mean and unit length by location and scale transformations. The center operator matrix is then

$$\mathbf{P} = \mathbf{I}_{N\times N} - \frac{\mathbf{1}}{\mathbf{N}}\mathbb{1}_{N\times N}, \tag{3.10}$$

where $\mathbf{I}_{N\times N}$ is an N-by-N identity matrix, $\mathbb{1}_{N\times N}$ is an N-by-N matrix of 1s. And the center transformation of $\mathbf{M}$ is

$$\mathbb{M} = \mathbf{P}\mathbf{M}, \tag{3.11}$$

where $\mathbb{M}_{ij} = \mathbf{M}_{ij} - \frac{1}{N}\sum_{k=0}^{N-1} \mathbf{M}_{kj}$. Let

$$\mathbf{U} = diag(\| \mathbb{M}_0 \|_2, \| \mathbb{M}_1 \|_2, \| \mathbb{M}_2 \|_2, \ldots, \| \mathbb{M}_{Q-1} \|_2,), \tag{3.12}$$

where $\| \mathbb{M}_j \|_2 = \sqrt{\sum_{i=0}^{N-1} \mathbb{M}_{ij}^2}$, and the unit transformation of $\mathbf{M}$ is

$$\mathbf{A} = \mathbb{M}\mathbf{U}^{-1}, \tag{3.13}$$

where $\mathbf{A}_{ij} = \mathbb{M}_{ij}/\sqrt{\sum_{k=0}^{N-1} \mathbb{M}_{kj}^2}$. Thus, the lasso ENZ AR model is

$$\min_{\mathbf{x}} \| \mathbf{A}\mathbf{x} - \mathbf{y} \|_2^2 + \mu \| \mathbf{x} \|_1, \tag{3.14}$$

where $\mathbf{x} = \mathbf{U}\boldsymbol{\beta}$ and $\mathbf{y} = \mathbf{P}\mathbf{L}$.

We adopt the adaptive method [4] to determine μ. The strategy for choosing regularization parameters in nonsmooth Tikhonov functional (3.14) is solely based on the value function of (3.14). The fixed point algorithm [4, Algorithm 1] for choosing regularization parameters balances the fidelity $\| \mathbf{A}\mathbf{x} - \mathbf{y} \|_2^2$ with the penalty $\| \mathbf{x} \|_1$. As suggested in [4], the initial value for μ is set to a small positive number and the input parameter γ of [4, Algorithm 1] is set to a tiny positive constant

number. The detailed description of the adaptive method is described in [4, Algorithm 1].

We propose Algorithm 2 for lasso ENZ AR based on the Bregman iterative algorithm [3]. Let $\mathbf{x} = SpaRSA(\mathbf{b}, \mathbf{A}, \mu)$ denote the output of the SpaRSA algorithm [31] for the constrained optimization problem $\min_{\mathbf{x}}\{\| \mathbf{Ax} - \mathbf{b} \|_2^2 + \mu \| \mathbf{x} \|_1\}$ with the inputs $\mathbf{b}$, $\mathbf{A}$, $\mu^{(0)}$, γ.

Algorithm 2. ENZ AR via lasso.

Input: the collected PSFs I_b, the maximum iteration step K, γ and $\mu^{(0)}$

Output: the variable vector $\widehat{\boldsymbol{\beta}}^{(K)}$

Main Procedure:

Initialization:
Set $C^{(0)} = 0$;
Form $\mathbf{W}$ by (A.23), (A.27), (A.30) and (A.33).
Form the matrix $\mathbf{H}$ by (A.25), (A.29), and (A.30).
$\mathbf{M} = \mathbf{WH}$.
Form $\mathbf{P}$ by (3.10).
$\mathbb{M} = \mathbf{PM}$.
Form $\mathbf{U}$ by (3.12).
$\mathbf{A} = \mathbb{M}\mathbf{U}^{-1}$.
for $k = 0, 1, 2, \ldots, K$ **do**
  $I_d^{(k)} \leftarrow I_b - C^{(k)}$.
  Form $\mathbf{z}^{(k)}$ from $I_d^{(k)}$ by (A.22), (A.26) and (A.30).
  $\mathbf{y}^{(k)} = \mathbf{PWz}^{(k)}$.
  $\mathbf{b}^{(0)} = \mathbf{y}^{(k)}$.
  for $j = 0, 1, 2\ldots, J$ **do**
    $\hat{\mathbf{x}}^{(j)} = SpaRSA(\mathbf{b}^{(j)}, \mathbf{A}, \mu^{(k)})$.
    $\mathbf{v} = \mathbf{Y}^{(k)} - \mathbf{A}\hat{\mathbf{x}}^{(j)}$.
    if $\| \mathbf{v} \|_2 < \varepsilon$ **then**
      break.
    end if
    $\mathbf{b}^{(j+1)} = \mathbf{b}^{(j)} + \mathbf{v}$.
  end for
  $\mu^{(k+1)} = \frac{\| \mathbf{v} \|_2^2}{\gamma \| \hat{\mathbf{x}}^{(k)} \|_1}$.
  $\widehat{\boldsymbol{\beta}}^{(k)} = \mathbf{U}^{-1}\hat{\mathbf{x}}^{(k)}$.
  Calculate $C^{(k+1)}$ by (2.7).
end for

4. Simulation

We compared Algorithm 2 with Algorithm 1 for the synthesized data, six common aberrations in optical systems, and simulated data. The characteristics of the optical system are shown in Table 1.

The simulations were implemented in three steps:

(1) We simulated three PSFs (images intra, in, and extra focus) from (2.6) with the first 91 leading terms, $\{\beta_m^m\}$. We added Gaussian white noise to them and simulated four noise levels (40 dB, 35 dB, 30 dB, and 25 dB) measured using signal–noise ratio (SNR).
(2) ENZ AR was used to estimate $\{\beta_n^m\}$ (by Algorithms 1 and 2 separately) using the simulated images. We set Q=91 in AR process. In the following experiments, we choose $\gamma = 0.01$ always, and $\mu^{(0)} = 1 \times 10^{-12}$ in Algorithm 2.
(3) It is easy to see that the generalized pupil functions generated by the two different parameter vectors $\boldsymbol{\beta}$ and $\alpha\boldsymbol{\beta}$, respectively, where α is constant, have the same phase. Thus in the following, $\{\widehat{\beta}_n^m\}$ is standardized by dividing by $\widehat{\beta}_0^0$ to ensure that the first component of $\{\widehat{\beta}_n^m\}$ is 1, and then comparing experimental results on residual square error, $\| \widehat{\boldsymbol{\beta}} - \boldsymbol{\beta} \|_2^2 / \| \boldsymbol{\beta} \|^2$, where $\boldsymbol{\beta}$ is the true parameter vector discussed above. We denote $\widehat{\boldsymbol{\beta}}$ to be obtained by Algorithms 1 and 2 separately.

Table 1
Characteristics of the optical system.

Light source diameter (μm)	0.25
Numerical aperture	0.5
Wavelength (μm)	0.2
Polar angle sampling (deg)	10
Polar radius sampling	$4pix/(\lambda F\#)$
Expected focus f (μm)	−1/0/1

Remark 1. Here we explain the reason for $\boldsymbol{\beta}$ and $\alpha\boldsymbol{\beta}$ having the same phase. Firstly, it is noted that the generalized pupil function is determined by (2.1). So the phase of each term in right hand of the generalized pupil is composed from $m\theta$ and the phase of the corresponding component of $\boldsymbol{\beta}$. When α is real, then $\boldsymbol{\beta}$ and $\alpha\boldsymbol{\beta}$ have the same phase. While α is complex number, $\boldsymbol{\beta}$ and $\alpha\boldsymbol{\beta}$ only difference with each other up to a constant phase, which is named piston in optics. Usually if two phases difference with each other in terms of piston, they can be viewed as having the same phase.

Different noise levels were chosen, and the above procedures were executed hundreds of time for each noise level. The estimated MSEs of $\boldsymbol{\beta}$ from Algorithms 1 and 2 were calculated by the following:

$$MSE = \frac{1}{N}\sum_{i=1}^{N} \| \widehat{\boldsymbol{\beta}}_i - \boldsymbol{\beta}_i \|_2^2, \tag{4.1}$$

$$STD = \sqrt{\frac{1}{N-1}\sum_{i=1}^{N} (\| \widehat{\boldsymbol{\beta}}_i - \boldsymbol{\beta}_i \|_2^2 - MSE)^2}, \tag{4.2}$$

where i means the ith test. N is the total number of test.

4.1. Random aberration examples

We used the method in [17] to generate 100 random phases ($pv < 2\pi$, $rms = 0.2\pi$ (rad)) by first 21 terms of Frits Zernike expansion. Some of them are shown in Fig. 1. These phases at constant amplitude generated 100 generalized pupils, which were then expressed by ENZ through (2.1), for Q=91 in ENZ. Then, we get 100 $\{\beta_n^m\}$ as the test data set. We compared the MSEs of outputs from Algorithms 1 and 2 for these random aberrations. The error bars are shown in Fig. 4, where each data point was the MSE (averaged over the 100 experimental results and calculated by (4.1)) at the given SNR, and the error bar is a distance of standard deviation of residual square errors (STD, calculated by (4.2)) above and below the curve so that each bar is symmetric and 2STD long. Algorithm 2 consistently produces a superior estimated parameter vector at those noise levels compared to Algorithm 1.

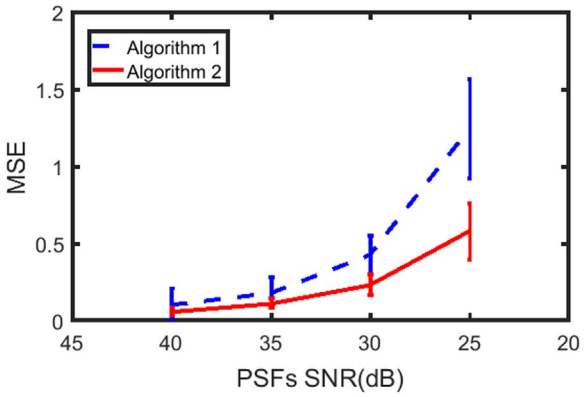

Fig. 4. The error bars of ENZ AR and lasso ENZ AR at different noise levels for 100 random aberrations.

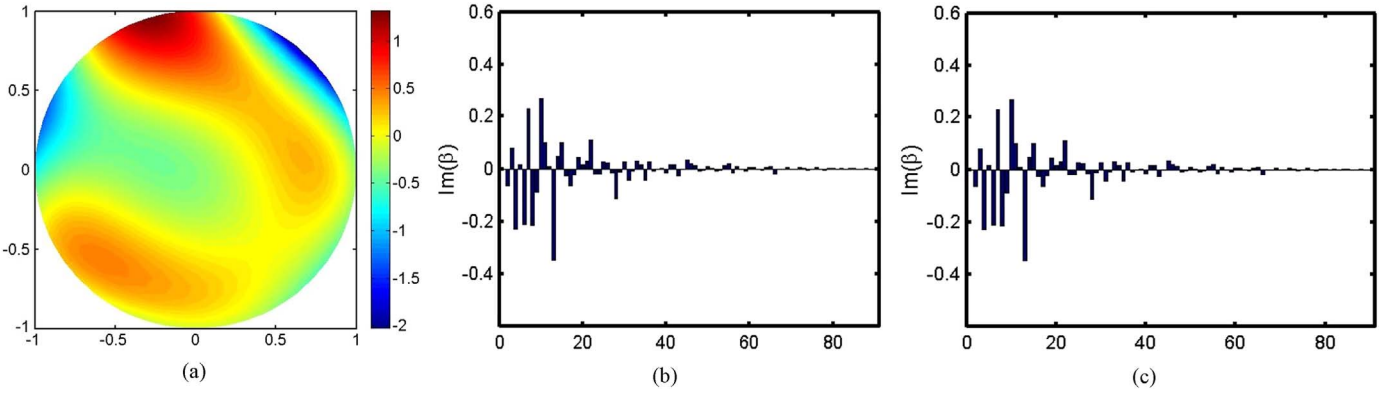

Fig. 5. Phase of non-common path aberrations and NZ coefficients (representing the field with constant amplitude and the given phases). (a) Phases. (b) Real part of NZ coefficients. (c) Imaginary part of NZ coefficients.

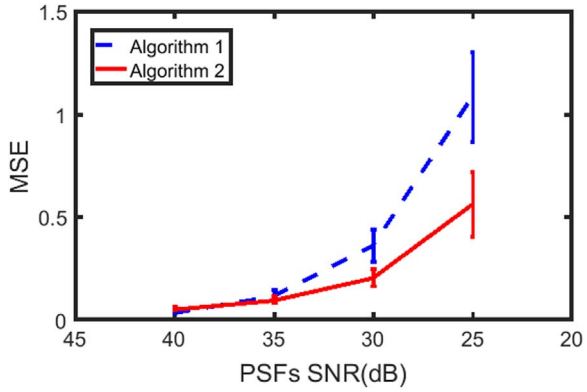

Fig. 6. The error bars of ENZ AR and lasso ENZ AR for different noise levels for the aberration shown in Fig. 5.

4.2. Simulation results for real aberration

The phase shown in Fig. 5a was observed from measurement of non-common path aberrations from a 1.23 m adaptive optics telescope in Changchun China. The NZ coefficients which can represent the field with constant amplitude and phase (Fig. 5a, $rms = 0.14\pi$ (rad)) are shown in Figs. 5b and c. We repeated the same simulations for ENZ AR and lasso ENZ AR, with error bars shown in Fig. 6. When the noise STD is 0.5, the original ENZ AR produces marginally improved estimated result. However, as STD increases, lasso ENZ AR performance immediately supersedes ENZ AR, and continues to provide improved estimates as STD continues to increase.

5. Conclusion

We highlighted that the ENZ coefficients to represent an optical field are sparse, and proposed lasso ENZ AR to model variable selection for ENZ AR, providing a reliable solution algorithm. Lasso ENZ AR shows two advantages over ENZ AR. The first is reforming the traditional empirical variable selection into an adaptive selection method, and numerical and real data examples validate that lasso ENZ AR provides improved estimation accuracy of the parameter vector.

Acknowledgments

The authors thank Prof. Zhouchen Lin for his valuable suggestions. Also we are indebted to the referee for his/her constructive comments, which helped us to improve the earlier version of this paper greatly. This work is supported by National Natural Science Foundation of China under Grant No. 11631003.

Appendix A. Linear least squares form for ENZ AR

If we neglect the cross-terms,

$$I_{appr}(r, \varphi; f) = I(r, \varphi; f) - C(r, \varphi; f), \tag{A.1}$$

we may assume that the noise $\varepsilon(r, \varphi; f)$ for each pixel of the imaging plane is Gaussian random, independent, and identical distributed, i.e., $\varepsilon(r, \varphi; f) \sim N(0, \sigma^2)$, where $N(0, \sigma^2)$ denotes a Gaussian distribution with mean 0 and variance σ^2. Let $I_b(r, \varphi; f)$ denote the measured PSF, then

$$I_b(r, \varphi; f) = I(r, \varphi; f) + \varepsilon(r, \varphi; f). \tag{A.2}$$

We define I_d:

$$I_d(r, \varphi; f) = I_{appr}(r, \varphi; f) + \varepsilon(r, \varphi; f), \tag{A.3}$$

and for two integral functions, we introduce the inner product [10]

$$\langle A, B\rangle = \int_{-\infty}^{+\infty}\int_{0}^{+\infty} A(r, f)B^*(r, f)rdrdf, \tag{A.4}$$

where $B^*(r, f)$ is the complex conjugate function of $B(r, f)$. If

$$\chi_n^m(r, f) = \begin{cases} 8Re[\mathbf{i}^m V_n^m(r, f)V_0^{0*}(r, f)], & \text{if } m = 0, \\ 4Re[\mathbf{i}^m V_n^m(r, f)V_0^{0*}(r, f)], & \text{if } m \neq 0, \end{cases} \tag{A.5}$$

$$\psi_n^m(r,f)=\begin{cases}-8Im[\mathbf{i}^m V_n^m(r,f)V_0^{0*}(r,f)], & \text{if } m=0,\\ -4Im[\mathbf{i}^m V_n^m(r,f)V_0^{0*}(r,f)], & \text{if } m\neq 0,\end{cases} \tag{A.6}$$

then $\langle \chi_n^m, \psi_{n'}^m\rangle = 0, \forall\ n, n'$, following [21].

Substituting (2.6) and (A.1) into (A.3), applying Fourier cosine transform to both sides, and operating the inner products with $\chi_n{}^m$ and $\psi_n{}^m$ respectively,

$$\begin{cases}\frac{1}{2}\langle\chi_0^0,\chi_{n'}^0\rangle(\beta_0^0)^2+\beta_0^0\sum_n{}'Re(\beta_n^0)\langle\chi_n^0,\chi_{n'}^0\rangle+\langle C\varepsilon^0,\chi_{n'}^0\rangle=\langle CI_d^0,\chi_{n'}^0\rangle,\\ \beta_0^0\sum_n{}'Im(\beta_n^0)\langle\psi_n^0,\psi_{n'}^0\rangle+\langle C\varepsilon^0,\psi_{n'}^0\rangle=\langle CI_d^0,\psi_{n'}^0\rangle,\end{cases}\quad m=0;\quad n,n'=0,2,\ldots \tag{A.7}$$

$$\begin{cases}\beta_0^0\sum_n[Re(\beta_n^m)+Re(\beta_n^{-m})]\langle\chi_n^m,\chi_{n'}^m\rangle+\langle C\varepsilon^m,\chi_{n'}^m\rangle=\langle CI_d^m,\chi_{n'}^m\rangle\\ \beta_0^0\sum_n[Im(\beta_n^m)+Im(\beta_n^{-m})]\langle\psi_n^m,\psi_{n'}^m\rangle+\langle C\varepsilon^m,\psi_{n'}^m\rangle=\langle CI_d^m,\psi_{n'}^m\rangle\end{cases} m=1,2,\ldots;\quad n,n'=m,m+2,\ldots \tag{A.8}$$

where

$$CI_d^m(r,f)=\frac{1}{2\pi}\int_0^{2\pi} I_d(r,\varphi;f)\cos(m\varphi)d\varphi, \tag{A.9}$$

$$C\varepsilon^m(r,f)=\frac{1}{2\pi}\int_0^{2\pi} \varepsilon(r,\varphi;f)\cos(m\varphi)d\varphi, \tag{A.10}$$

$$\left\langle C\varepsilon^m,\chi_{n'}^m\right\rangle\sim\begin{cases}N\left(0,\frac{\sigma^2}{2\pi}\Delta_\varphi\langle 1,\chi_{n'}^m\rangle^2\right), & \text{if } m=0 \text{ or } m=\pi/\Delta_\varphi,\\ N\left(0,\frac{\sigma^2}{4\pi}\Delta_\varphi\langle 1,\chi_{n'}^m\rangle^2\right), & \text{others},\end{cases} \tag{A.11}$$

$$\langle C\varepsilon^m,\psi_{n'}^m\rangle\sim\begin{cases}N\left(0,\frac{\sigma^2}{2\pi}\Delta_\varphi\langle 1,\psi_{n'}^m\rangle^2\right), & \text{if } m=0 \text{ or } m=\pi/\Delta_\varphi,\\ N\left(0,\frac{\sigma^2}{4\pi}\Delta_\varphi\langle 1,\psi_{n'}^m\rangle^2\right), & \text{others},\end{cases} \tag{A.12}$$

where Δ_φ is the sampling step of φ on the focal-plane.

Similarly, if we apply Fourier sine transform,

$$\begin{cases}-\beta_0^0\sum_n[Im(\beta_n^m)-Im(\beta_n^{-m})]\langle\chi_n^m,\chi_{n'}^m\rangle+\langle S\varepsilon^m,\chi_{n'}^m\rangle=\langle SI_d^m,\chi_{n'}^m\rangle\\ \beta_0^0\sum_n[Re(\beta_n^m)-Re(\beta_n^{-m})]\langle\psi_n^m,\psi_{n'}^m\rangle+\langle S\varepsilon^m,\psi_{n'}^m\rangle=\langle SI_d^m,\psi_{n'}^m\rangle\end{cases} m=1,2,\ldots;\quad n,n'=m,m+2,\ldots \tag{A.13}$$

where

$$SI_d^m(r,f)=\frac{1}{2\pi}\int_0^{2\pi} I_d(r,\varphi;f)\sin(m\varphi)d\varphi, \tag{A.14}$$

$$S\varepsilon^m(r,f)=\frac{1}{2\pi}\int_0^{2\pi} \varepsilon(r,\varphi;f)\sin(m\varphi)d\varphi, \tag{A.15}$$

$$\left\langle S\varepsilon^m,\chi_{n'}^m\right\rangle\sim N\left(0,\frac{\sigma^2}{4\pi}\Delta_\varphi\langle 1,\chi_{n'}^m\rangle^2\right),\quad \text{if } m\neq 0 \text{ and } m\neq\pi/\Delta_\varphi, \tag{A.16}$$

$$\langle S\varepsilon^m,\chi_{n'}^m\rangle=0,\quad \text{if } m=0 \text{ or } m=\pi/\Delta_\varphi, \tag{A.17}$$

$$\langle S\varepsilon^m,\psi_{n'}^m\rangle\sim N\left(0,\frac{\sigma^2}{4\pi}\Delta_\varphi\langle 1,\psi_{n'}^m\rangle^2\right),\quad \text{if } m\neq 0 \text{ and } m\neq\pi/\Delta_\varphi, \tag{A.18}$$

$$\langle S\varepsilon^m,\psi_{n'}^m\rangle=0,\quad \text{if } m=0 \text{ or } m=\pi/\Delta_\varphi. \tag{A.19}$$

Since $0<m<\pi/\Delta_\varphi$ in (A.13), (A.17) and (A.19) will not appear in (A.13).

Since we use only the first Q terms in ENZ expansion, let us introduce the symbol $\lceil\frac{n_{max}+1-k}{2}\rceil$ to denote the cardinality of the set $\{a|V_a^k \text{ exists and } a\le n_{max}\}$, and define

$$T_m=\begin{cases}0, & \text{if } m=1,\\ 2\sum_{k=0}^{m}\left\lceil\frac{n_{max}+1-k}{2}\right\rceil, & \text{if } m\le 0,\end{cases} \tag{A.20}$$

$$n_{max}=gn(Q), \tag{A.21}$$

where m_{max} is the absolute maximum of m in the first Q terms of the ENZ expansion.

First, let $\mathbf{H_C}\in R^{T_{m_{max}}\times(2Q-1)}$, $\mathbf{z_C}\in R^{T_{m_{max}}}$, and $\boldsymbol{\varepsilon_C}\in R^{T_{m_{max}}}$. Set $\mathbf{H_C}=0$ and for $m=0,1,2,\ldots,m_{max}$, let

$$\mathbf{z_C}[i] = \begin{cases} \langle CI_d^m, \chi_{i+m-T_{m-1}}^m \rangle, & \text{if } T_{m-1} \le i < T_m \text{ and } i \text{ is even}, \\ \langle CI_d^m, \psi_{i+m-T_{m-1}}^m \rangle, & \text{if } T_{m-1} \le i < T_m \text{ and } i \text{ is odd}, \end{cases} \tag{A.22}$$

$$\boldsymbol{\omega_C}[i] = \begin{cases} \sqrt{\dfrac{\Delta_\varphi}{2\pi}} |\langle 1, \chi_{i+m-T_{m-1}}^m \rangle|, & \text{if } m = 0 \text{ and } T_{m-1} \le i < T_m \text{ and } i \text{ is even}, \\ \sqrt{\dfrac{\Delta_\varphi}{4\pi}} |\langle 1, \chi_{i+m-T_{m-1}}^m \rangle|, & \text{if } m \ne 0 \text{ and } T_{m-1} \le i < T_m \text{ and } i \text{ is even}, \\ \sqrt{\dfrac{\Delta_\varphi}{4\pi}} |\langle 1, \psi_{i+m-T_{m-1}}^m \rangle|, & \text{if } T_{m-1} \le i < T_m \text{ and } i \text{ is odd}, \end{cases} \tag{A.23}$$

$$\boldsymbol{\varepsilon_C}[i] \sim N(0, \sigma^2(\boldsymbol{\omega_C}[i])^2) \quad T_{m-1} \le i < T_m, \tag{A.24}$$

$$\mathbf{H_C}[i,j] = \begin{cases} \dfrac{1}{2}\langle \chi_{gn(j)}^{gm(j)}, \chi_{i+m-T_{m-1}}^m \rangle, & \text{if } \begin{matrix} m = 0 \text{ and } 0 \le j < Q, \ gm(j) = m \\ \text{and } T_{m-1} \le i < T_m \text{ and } i \text{ is even}, \end{matrix} \\ \langle \chi_{gn(j)}^{gm(j)}, \chi_{i+m-T_{m-1}}^m \rangle, & \text{if } \begin{matrix} \text{if } m \ne 0 \text{ and } 0 \le j < Q, \ |gm(j)| = m \\ \text{and } T_{m-1} \le i < T_m \text{ and } i \text{ is even}, \end{matrix} \\ \langle \psi_{gn(j-Q+1)}^{gm(j-Q+1)}, \psi_{i+m-T_{m-1}}^m \rangle, & \text{if } \begin{matrix} \text{if } Q \le j < 2Q-1, \ \text{ and } |gm(j-Q+1)| = m \\ \text{and } T_{m-1} \le i < T_m \text{ and } i \text{ is odd}, \end{matrix} \end{cases} \tag{A.25}$$

Second, we introduce the matrix $\mathbf{H_S} \in R^{(T_{m_{max}}-T_0)\times(2Q-1)}$, and vectors $\mathbf{Z_S} \in R^{T_{m_{max}}-T_0}$ and $\boldsymbol{\varepsilon_S} \in R^{T_{m_{max}}-T_0}$. Set $\mathbf{H_S} = 0$ and for $m = 1, 2, \ldots, m_{max}$, let

$$\mathbf{z_S}[i] = \begin{cases} \langle SI_d^m, \chi_{i+m-T_{m-1}}^m \rangle, & \text{if } T_{m-1} - T_0 \le i < T_m - T_0 \text{ and } i \text{ is even}, \\ \langle SI_d^m, \psi_{i+m-1-T_{m-1}}^m \rangle, & \text{if } T_{m-1} - T_0 \le i < T_m - T_0 \text{ and } i \text{ is odd}, \end{cases} \tag{26}$$

$$\boldsymbol{\omega_S}[i] = \begin{cases} \sqrt{\dfrac{\Delta_\varphi}{4\pi}} |\langle 1, \chi_{i+m-T_{m-1}}^m \rangle|, & \text{if } T_{m-1} - T_0 \le i < T_m - T_0 \text{ and } i \text{ is even}, \\ \sqrt{\dfrac{\Delta_\varphi}{4\pi}} |\langle 1, \psi_{i+m-1-T_{m-1}}^m \rangle|, & \text{if } T_{m-1} - T_0 \le i < T_m - T_0 \text{ and } i \text{ is odd}, \end{cases} \tag{27}$$

$$\boldsymbol{\varepsilon_S}[i] \sim N(0, \sigma^2(\boldsymbol{\omega_S}[i])^2) \quad T_{m-1} - T_0 \le i < T_m - T_0, \tag{28}$$

$$\mathbf{H_S}[i,j] = \begin{cases} -\langle \chi_{gn(j-Q+1)}^{gm(j-Q+1)}, \chi_{i+m-T_{m-1}}^m \rangle, & \text{if } \begin{matrix} Q \le j < 2Q-1 \text{ and } gm(j-Q+1) = m \\ \text{and } T_{m-1} - T_0 \le i < T_m - T_0 \text{ and } i \text{ is even}, \end{matrix} \\ \langle \chi_{gn(j+1)}^{gm(j+1)}, \chi_{i+m-T_{m-1}}^m \rangle, & \text{if } \begin{matrix} Q \le j < 2Q-1 \text{ and } gm(j-Q+1) = -m \\ \text{and } T_{m-1} - T_0 \le i < T_m - T_0 \text{ and } i \text{ is even}, \end{matrix} \\ \langle \psi_{gn(j+1)}^{gm(j+1)}, \psi_{i+m-1-T_{m-1}}^m \rangle, & \text{if } \begin{matrix} 0 \le j < Q \text{ and } gm(j+1) = m \text{ and} \\ T_{m-1} - T_0 \le i < T_m - T_0 \text{ and } i \text{ is odd}, \end{matrix} \\ -\langle \psi_{gn(j+1)}^{gm(j+1)}, \psi_{i+m-1-T_{m-1}}^m \rangle, & \text{if } \begin{matrix} 0 \le j < Q \text{ and } gm(j+1) = -m \text{ and} \\ T_{m-1} - T_0 \le i < T_m - T_0 \text{ and } i \text{ is odd}, \end{matrix} \end{cases} \tag{29}$$

Finally, let

$$\mathbf{z} = \begin{bmatrix} \mathbf{z_C} \\ \mathbf{z_S} \end{bmatrix}, \quad \boldsymbol{\varepsilon} = \begin{bmatrix} \boldsymbol{\varepsilon_C} \\ \boldsymbol{\varepsilon_S} \end{bmatrix}, \quad \boldsymbol{\omega} = \begin{bmatrix} \boldsymbol{\omega_C} \\ \boldsymbol{\omega_S} \end{bmatrix}, \quad \mathbf{H} = \begin{bmatrix} \mathbf{H_C} \\ \mathbf{H_S} \end{bmatrix}, \tag{A.30}$$

and (A.7), (A.8) and (A.13) can be expressed as the linear system

$$\mathbf{H}\boldsymbol{\beta} + \boldsymbol{\varepsilon} = \mathbf{z}, \tag{A.31}$$

where

$$\boldsymbol{\beta}[i] = \begin{cases} (\beta_0^0)^2, & \text{if } i = 0, \\ \beta_0^0 \times Re(\beta_{gn(i)}^{gm(i)}), & \text{if } 0 < i \le Q-1, \\ \beta_0^0 \times Im(\beta_{gn(i)}^{gm(i)}), & \text{if } Q-1 < i \le 2Q-2. \end{cases} \tag{A.32}$$

To ensure each component of the random vector has the same variance, we introduce the weighted matrix

$$\mathbf{W} = (diag(\boldsymbol{\omega} + \tau\mathbf{1}))^{-1}, \tag{A.33}$$

where $diag(u)$ is a diagonal matrix with $diag(u)_{ii} = u_i$, $\mathbf{1}$ is a vector with each component being 1 and τ is a very small real value such that each component of $\boldsymbol{\omega} + \tau\mathbf{1}$ is nonzero. Left multiplying both sides of (A.31),

$$\mathbf{M}\boldsymbol{\beta} + \boldsymbol{\delta} = \mathbf{L}, \tag{A.34}$$

where $\mathbf{L} = \mathbf{W}\mathbf{z}, \boldsymbol{\delta} = \mathbf{W}\boldsymbol{\varepsilon}, \mathbf{M} = \mathbf{W}\mathbf{H}$. The matrix $\mathbf{M}$ is called the covariate matrix [22], and has dimension $2Q \times (2Q-1)$, since Q is small. Thus, we can solve (A.34) with low computation costs by linear least squares:

$$\widehat{\boldsymbol{\beta}} = \arg\min_{\boldsymbol{\beta}} \| \mathbf{M}\boldsymbol{\beta} - \mathbf{L} \|_2^2 = (\mathbf{M}^T\mathbf{M})^{-1}\mathbf{M}^T\mathbf{L}. \tag{A.35}$$

References

[1] L. Bregman, The relaxation method of finding the common points of convex sets and its application to the solution of problems in convex programming, USSR Comput. Math. Math. Phys. 7 (1967) 1208–1229.

[2] J.F. Cai, S. Osher, Z. Shen, Linearized Bregman iterations for compressed sensing, Math. Comput. 78 (267) (2008) 1515–1536.

[3] W. Yin, S. Osher, D. Goldfarb, J. Darbon, Bregman iterative algorithms for l1-minimization with applications to compressed sensing, SIAM J. Imaging Sci. 1 (1) (2008) 143–168.

[4] K. Ito, B. Jin, T. Takeuchi, A regularization parameter for nonsmooth Tikhonov regularization, SIAM J. Sci. Comput. 33 (3) (2011) 1415–1438.

[5] A.J.E.M. Janssen, Extended Nijboer–Zernike approach for the computation of optical point-spread functions, J. Opt. Soc. Am. A 19 (5) (2002) 849–857.

[6] P. Braat, J.J.M. Dirksen, A.J.E.M. Janssen, Assessment of an extended Nijboer–Zernike approach for the computation of optical point-spread functions, J. Opt. Soc. Am. A 19(5) (2002) 858–870.

[7] X.Y. Liu, L. Wang, J.L. Wang, H.R. Meng, A three-dimensional point spread function for phase retrieval and deconvolution, Opt. Express 20 (14) (2012) 15393.

[8] J.J.M. Braat, P. Dirksen, A.J.E.M. Janssen, A.S. van de Nes, Extended Nijboer–Zernike representation of the vector field in the focal region of an aberrated high aperture optical system, J. Opt. Soc. Am. A 20 (2003) 2281–2292.

[9] P. Braat, J.J.M. Dirksen, A.J.E.M. Janssen, S. van Haver, A.S. van de Nes, Extended Nijboer–Zernike approach to aberration and birefringence retrieval in a high-numerical-aperture optical system, J. Opt. Soc. Am. A 22 (2005) 2635–2650.

[10] P. Dirksen, J.J.M. Braat, A.J.E.M. Janssen, C.A.H. Juffermans, Aberration retrieval using the extended Nijboer–Zernike approach, J. Microlith. Microfab. Microsyst. 2 (2003) 61–68.

[11] P. Dirksen, J.J.M. Braat, A.J.E.M. Janssen, Estimating resist parameters in optical lithography using the extended Nijboer–Zernike theory, J. Microlith. Microfab. Microsyst. 5 (1) (2006) 013005.

[12] P. Riaud, D. Mawet, A. Magette, Nijboer–Zernike phase retrieval for high contrast imaging principle, on-sky demonstration with NACO, and perspectives in vector vortex coronagraphy, Astron. Astrophys. 545 (2012) A150.

[13] Jacopo Antonello, Michel Verhaegen, Modal-based phase retrieval for adaptive optics, J. Eur. Opt. Soc. 32 (2015) 1160–1170.

[14] S. Wang, J. Shi, J. Yin, M. Xia, Introduction of Linear Model, Science Publisher, Beijing, 2004 (in Chinese).

[15] S. van Haver, A.J.E.M. Janssen, Advanced analytic treatment and efficient computation of the diffraction integrals in the extended Nijboer–Zernike theory, J. Eur. Opt. Soc. Rapid Publ. 8 (2013) 13044.

[16] Anat Levin, Yair Weiss, User assisted separation of reflections from a single image using a sparsity prior, IEEE Trans. Pattern Anal. Mach. Intell. 29 (9) (2007) 1647–1654.

[17] A. Nicolas, Roddier atmospheric wavefront simulation using Zernike polynomials, Opt. Eng. 29 (10) (1990) 1174–1180.

[18] T. Hastie, R. Tibshirani, J. Friedman, The Elements of Statistical Learning, Springer, Heidelberg, 2009.

[19] R. Tibshirani, Regression shrinkage and selection via the lasso, J. R. Stat. Soc. B 58 (1) (1996) 267–288.

[20] S. van Haver, J.J.M. Braat, P. Dirksen, A.J.E.M. Janssen, High-NA aberration retrieval with the extended Nijboer–Zernike vector diffraction, J. Eur. Opt. Soc. 1 (2006) 06004.

[21] J.J.M. van der Avoort, J.J.M. Braat, P. Dirksen, A.J.E.M. Janssen, Aberration retrieval from the intensity point-spread function in the focal region using the extended Nijboer–Zernike approach, J. Mod. Opt. 52(12) (2005) 1695–1728.

[22] B. Efron, T. Hastie, I. Johnstone, R. Tibshirani, Least angle regression, Ann. Stat. 32 (2) (2004) 407–499.

[23] T. Bonesky, Morozovs discrepancy principle and Tikhonov-type functionals, Inverse Probl. 25 (2009) 015015.

[24] B. Jin, J. Zou, Iterative Parameter Choice by Discrepancy Principle, Technical Report, Department of Mathematics, Chinese University of Hong Kong, Hong Kong, 2010.

[25] B. Jin, D.A. Lorenz, Heuristic parameter-choice rules for convex variational regularization based on error estimates, SIAM J. Numer. Anal. 48 (3) (2010) 1208–1229.

[26] Rick Chartrand, Wotao Yin, Iteratively reweighted algorithms for compressive sensing, in: 33rd International Conference on Acoustics, Speech, and Signal Processing (ICASSP), 2008.

[27] M.R. Hestenes, Multiplier and gradient methods, J. Optim. Theory Appl. 4 (5) (1969) 303–320. http://dx.doi.org/10.1007/BF009276731969.

[28] M.J.D. Powell, A method for nonlinear constraints in minimization problems, in: Optimization, Symposium, University of Keele, Keele, 1968, Academic Press, London, 1969, pp. 283–298.

[29] M. Figueiredo, R. Nowak, S.J. Wright, Gradient projection for sparse reconstruction: application to compressed sensing and other inverse problems, IEEE J. Sel. Top. Signal Process.: Spec. Issue Convex Optim. Methods Signal Process. 4 (1) (2007) 586–597.

[30] E.T. Hale, W. Yin, Y. Zhang, Fixed-point continuation for l1-minimization: methodology and convergence, SIAM J. Opt. 19 (3) (2008) 1107–1130.

[31] S.J. Wright, R.D. Nowak, M.A.T. Figueiredo, Sparse reconstruction by separable approximation, IEEE Trans. Signal Process. 57 (3) (2009) 2479–2493.